Proc. Natl. Acad. Sci. USA
Vol. 93, pp. 4937–4941, May 1996
Biophysics

Two-dimensional protein crystallization via metal-ion coordination by naturally occurring surface histidines

WOLFGANG FREY*, WILLIAM R. SCHIEF, JR.*, DANIEL W. PACK†, CHAO-TSEN CHEN†, ASHUTOSH CHILKOTI*, PATRICK STAYTON*, VIOLA VOGEL*‡, AND FRANCES H. ARNOLD†‡

*Center for Bioengineering, Box 357962, University of Washington, Seattle, WA 98195; and †Division of Chemistry and Chemical Engineering 210-41, California Institute of Technology, Pasadena, CA 91125

Communicated by Charles R. Cantor, Boston University, Boston, MA, December 28, 1995 (received for review November 13, 1995)

ABSTRACT **A powerful and potentially general approach to the targeting and crystallization of proteins on lipid interfaces through coordination of surface histidine residues to lipid-chelated divalent metal ions is presented. This approach, which should be applicable to the crystallization of a wide range of naturally occurring or engineered proteins, is illustrated here by the crystallization of streptavidin on a monolayer of an iminodiacetate-Cu(II) lipid spread at the air–water interface. This method allows control of the protein orientation at interfaces, which is significant for the facile production of highly ordered protein arrays and for electron density mapping in structural analysis of two-dimensional crystals. Binding of native streptavidin to the iminodiacetate-Cu lipids occurs via His-87, located on the protein surface near the biotin binding pocket. The two-dimensional streptavidin crystals show a previously undescribed microscopic shape that differs from that of crystals formed beneath biotinylated lipids.**

The two-dimensional (2D) crystallization of proteins on lipid monolayers has become a powerful technique with diverse applications in fields ranging from structural biology to materials science. Protein 2D crystals have been used for structure determination via electron diffraction (1, 2) and for the seeding and epitaxial growth of three-dimensional protein crystals (3, 4). Furthermore, 2D protein crystals could form the basic structure of biosensors and opto-electronic devices or act as a template for the synthesis of novel organic and inorganic materials. However, the range of soluble proteins that might be crystallized in two dimensions has been limited due to the lack of a general method for addressing proteins to lipid interfaces.

A number of proteins have been crystallized at interfaces by targeting to surface-bound affinity ligands (1, 5), by electrostatic interactions (6), and by metal coordination by polyhistidine-tagged proteins (7). The first approach requires synthesis of a lipid displaying an appropriate affinity ligand (8–10). Furthermore, for many interesting proteins no convenient affinity ligand is known. Electrostatic attraction may be successful when the protein's surface charge distribution promotes adsorption with a unique orientation at the interface, but this approach is not general, and the protein orientation is difficult to predict. Kubalek *et al.* (10) recently described the 2D crystallization of polyhistidine-tagged HIV-reverse transcriptase on a monolayer of chelating lipids complexed to Ni^{2+}. Polyhistidine fusion peptides, widely used for purification of recombinant proteins by immobilized metal-affinity chromatography (IMAC) (11), provide a convenient mechanism for targeting recombinant proteins to lipid interfaces (12, 13). While this approach represents a valuable move toward more general crystallization methods, the peptide tag at the N or C terminus of the engineered protein imposes restrictions on the 2D crystal morphology and limits application to recombinant proteins successfully expressed with the polyhistidine sequence. A general method by which water-soluble proteins can be targeted, oriented, and crystallized at interfaces is highly desirable.

In contrast to the binding interactions described above, coordination to Cu^{2+}-chelating lipids by naturally occurring solvent-exposed histidine residues offers a potentially general approach to the crystallization of proteins at the air–water interface. This approach can be exploited with the very large number of native proteins that display histidines on their surfaces. Furthermore, the ability to engineer histidine residues at precise locations on the protein surface would allow control over protein orientation and 2D crystal morphology, useful for the structural analysis of 2D crystals as well as for applications in materials science and design of molecular devices.

We show here that naturally occurring surface histidines can be utilized to bind and crystallize the protein streptavidin on a monolayer of iminodiacetate-Cu^{2+} (IDA-Cu) lipids. Metal-affinity chromatography on an IDA-Cu column shows that protein interaction with IDA-Cu at neutral pH is generally limited to metal coordination by surface-accessible histidine residues ($K_a \approx 10^{3.5}$ M^{-1} for imidazole or a single surface histidine); at higher pH additional basic groups (lysine, N terminus) can also participate (14). We have previously shown by ESR and diethylpyrocarbonate modification that native proteins are targeted to IDA-Cu lipid assemblies through coordination by surface histidines (15).

Streptavidin is a tetrameric protein (M_r = 60,000) that binds the small molecule biotin, also known as vitamin H, with high affinity ($K_a \approx 10^{15}$ M^{-1}). The three-dimensional structure of streptavidin has been well characterized (16–19), and the protein is known to crystallize two dimensionally beneath monolayers of biotinylated lipids (20). 2D crystallization of streptavidin has also been induced by electrostatic interactions with a monolayer of poly(1-benzyl-L-histidine) (6). Streptavidin contains two surface-accessible histidine residues per subunit at positions 87 and 127 (18, 19), which, combined with the available structural information, make streptavidin an attractive model system for investigating this 2D crystallization approach.

MATERIALS AND METHODS

Streptavidin Mutants. The H87A and H127C streptavidin mutants were created by site-directed cassette mutagenesis of a synthetic "core" streptavidin gene encoding residues 13–139 of native streptavidin (21). Oligodeoxyribonucleotides spanning the *Mlu*I-*Hin*dIII and *Bsp*EI-*Msc*I restriction sites were

The publication costs of this article were defrayed in part by page charge payment. This article must therefore be hereby marked "*advertisement*" in accordance with 18 U.S.C. §1734 solely to indicate this fact.

Abbreviations: 2D, two dimensional; IDA, iminodiacetate; IMAC, immobilized metal-affinity chromatography; BAM, Brewster angle microscope; DOIDA, 1,2-dioleyl-*rac*-glycero-3-(8-(3,6-dioxy)octyl-1-amino-*N*,*N*-diacetic acid).

‡To whom reprint requests should be addressed. e-mail for F.H.A.: frances@macpost.caltech.edu; e-mail for V.V.: vogel@bioeng.washington.edu.

used for the H127C (22) and H87A mutations, respectively. The mutant sequences were confirmed with automated DNA sequencing and subsequently subcloned into pET-21a (Novagen) for expression in *Escherichia coli* BL21(DE3). Procedures used for expression, refolding, and purification of the mutants are those described previously for recombinant wild-type streptavidin (21).

Langmuir Trough and Solutions. The experiments were performed at room temperature in a Langmuir trough 5–6 mm deep and equipped with two movable barriers. The surface pressure and the movement of the barriers are computer controlled. The subphase for all experiments contained a buffer of 20 mM Mops and 250 mM NaCl (all from Sigma) at pH 7.8. The buffer was shaken with chloroform to remove organic contamination. After the phases had separated, the aqueous part was shaken with hexane to extract traces of chloroform. Core streptavidin (Boehringer Mannheim) was dissolved in the buffer described above. The protein concentration was determined by absorption spectroscopy at 280 nm with an absorption coefficient for the protein of 136,000 $M^{-1}\cdot cm^{-1}$. The monolayer experiments were performed under argon atmosphere to prevent oxidation of the unsaturated alkyl chains. After spreading, the lipid was compressed to a surface pressure of 3 mN/m, and the protein solution was injected between the barriers through the surface into the subphase with a micropipettor. The final protein concentration in the trough was about 8 μg/ml (≈150 nM). Injection of either EDTA (Aldrich) or biotin (Boehringer Mannheim) was performed with a micropipettor behind the barriers.

Brewster Angle Microscopy. The home-built Brewster angle microscope (BAM) is mounted above the Langmuir trough (see Fig. 2). The incoming He-Ne laser light of 10 mW is *p*-polarized by a Glan–Thompson polarizer (intensity ratio, 10^{-5}) at an angle of incidence of 53.12° with respect to the surface normal (Brewster angle for the air–water interface). The intensity reflected from the plain air–water interface at the Brewster angle is at the detection limit. The light reflected under *p*-polarization is collected by a lens system to form an image on a charge-coupled device camera. Because the BAM signal intensity is highly dependent on the water level, this was maintained automatically at a constant height by a home-built level control. The absolute intensity of reflected *p*-polarized light was stable and reproducible from experiment to experiment to within 1%.

Metal-Affinity Chromatography. The IMAC column (TSK Chelate-G6000XL, 7.5 cm × 7.5 mm; TosoHaas, Montgomeryville, PA) was regenerated and loaded with Cu^{2+} (23) and subsequently equilibrated with 10 ml of 50 mM sodium phosphate/0.5 M NaCl/100 mM imidazole, pH 7.8, followed by 10 ml of the same buffer containing 1 mM imidazole. Experiments were performed at a flow rate of 1 ml/min. After injecting protein (150 μl of 20 μM streptavidin) the column was washed with 6 ml of buffer containing 1 mM imidazole. The protein was then eluted with a linear gradient of imidazole from 1 to 100 mM over 114 ml, and the eluent was monitored by absorbance at 280 nm. The chromatograms have been corrected for the changing baseline due to absorbance of imidazole by subtraction of the trace obtained in the absence of protein.

RESULTS AND DISCUSSION

The surface active metal chelator DOIDA [1,2-dioleyl-*rac*-glycero-3-(8-(3,6-dioxy)octyl-1-amino-*N*,*N*-diacetic acid)] (Fig. 1) was designed especially for 2D protein crystallization. The IDA headgroup is attached to the glycerol backbone through a long (≈11.5 Å) triethylene glycol spacer to allow the metal–ion complex free access to the subphase. Tridentate IDA chelates divalent metal ions very tightly [$K_a \approx 10^{11}$ M^{-1} for Cu^{2+} (24)], leaving coordination sites available for ligand

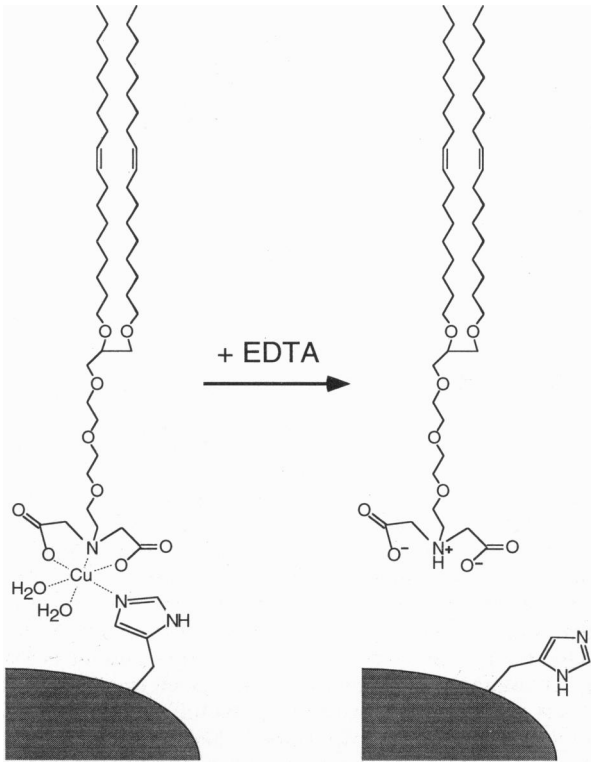

FIG. 1. Structure of the Cu(II)-chelating lipid DOIDA and its complex with a surface histidine. Addition of the soluble chelator EDTA removes Cu(II) and disrupts the ternary lipid–metal ion–protein complex.

binding, as illustrated in Fig. 1. Furthermore, the hydrophilic nature of the IDA–metal complex confers necessary amphiphilic character without incorporating ionic groups that can participate in nonspecific electrostatic interactions with proteins. The unsaturated dioleyl tails ensure the stability and fluidity of DOIDA Langmuir monolayers.

The DOIDA-Cu lipid was synthesized according to the sequence outlined in Fig. 2. Details of the synthesis will be presented elsewhere. The DOIDA glycerol backbone connects two ether-linked oleyl tails at positions 2 and 3 and a hydrophilic spacer to the chelating IDA headgroup on position 1. The trityl-protected glycerol **2** (prepared from glycerol **1**) and oleyl mesylate **4** (prepared from oleyl alcohol **3**) were coupled to produce **5**. Deprotection of the trityl group and esterification with 1-(methylsulfonyl)-9-(triphenylcarbinyl)-3,6,9-trioxynonane, prepared from triethylene glycol, introduced the triethylene glycol spacer group to the main lipid body (**7**). Subsequent functional group manipulation at the head group position according to modified procedures by Ng *et al.* (12) gave the iminodiacetic acid functionality. The DOIDA lipid was metalated by addition of a slight molar excess (<10%) of $CuCl_2$ dissolved in MeOH to the lipid solution in $CHCl_3$.

DOIDA forms stable monolayers at the air–water interface, both in the presence and absence of metal ions, and remains in the fluid state over a wide range of surface pressures due to the unsaturated lipid tails (unpublished results). For crystallization studies, the chelating lipid was loaded with Cu^{2+} before spreading of the Langmuir monolayer. Surface pressure-area isotherms of the pre-metallated lipid on buffered subphase in the absence of divalent metal ions were identical to the unmetalated lipid spread on the same subphase containing 1–10 mM $CuCl_2$, indicating that the metal ion is not lost to the subphase. Preloading of the lipid with metal was required, as Cu^{2+} in solution was found to inhibit binding and crystallization of the protein even under a biotinylated monolayer.

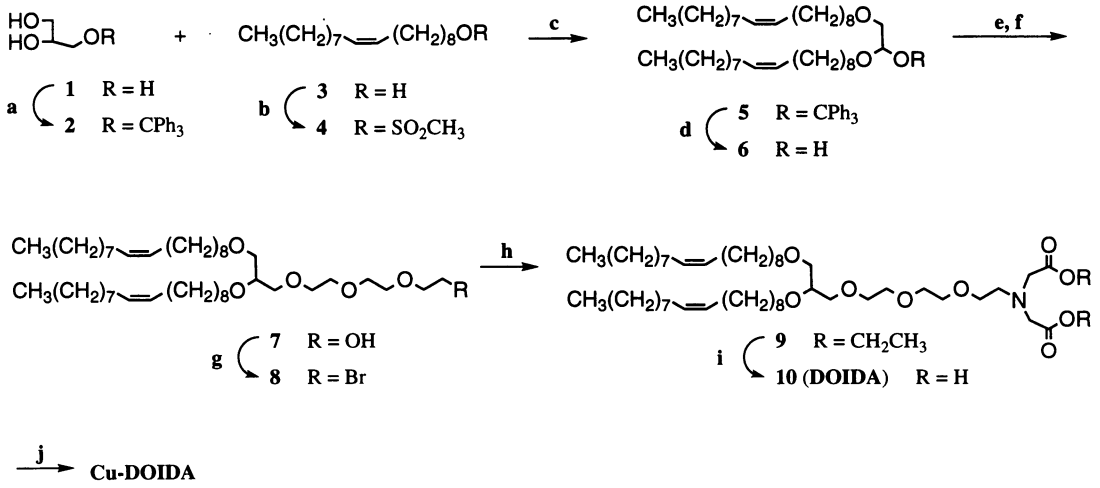

FIG. 2. Synthesis of DOIDA-Cu. Step a: trityl chloride 4-dimethylaminopyridine (DMAP), ET_3N, tetrahydrofuran (THF), 12 hr. Step b: methanesulfonyl chloride (MsCl), CH_2Cl_2, Et_3M, 12 hr. Step c: powered KOH, dimethyl sulfoxide, 80°C, 36 hr. Step d: TsOH, THF/CH_3OH, room temperature, 12 hr. Step e: NaH, 1-(methylsulfonyl)-9-(triphenylcarbinyl)-3.6.9-trioxynonane, THF, reflux, 12 hr. Step f: TsOH, THF/CH_3OH, room temperature, 12 hr. Step g: CBr_4, PPh_3, THF, 0°C to room temperature, 12 hr. Step h: diethyliminodiacetate, Et_3N, THF, 72 hr. Step i: NaOH, THF/CH_3OH/H_2O, reflux, 1 hr. Step j: $CuCl_2$, $CH_3OH/CHCl_3$, 1 hr.

The surface adsorption and crystallization of streptavidin is visualized by BAM, a recently developed optical microscopy technique that allows imaging of molecular monolayers under Brewster's angle (25, 26). A schematic of BAM is shown in Fig. 3*a*. The bare water interface produces no reflection of *p*-polarized light incident at Brewster's angle. When a covering layer even as thin as a molecular monolayer is introduced, *p*-polarized light is reflected and an image can be created. In contrast to fluorescence microscopy, photolabeling of the protein is not necessary because the signal intensity of the BAM images increases with the layer thickness and the refractive index of the interfacial film. It was recently demonstrated (27) that BAM allows the visualization of surface adsorption and aggregation of proteins and that a quantitative analysis of the image gray scale can provide a laterally resolved measure of protein surface density.

A representative BAM image of 2D biotin lipid-bound streptavidin aggregates at the air–water interface, which are known from the literature to be crystalline (3, 20), is shown in Fig. 3*b*. Bright H-shaped crystals can be seen on a dark background. A gray scale analysis of this image shows that protein is bound not only within the crystals but fills the space between crystals as well. The crystalline protein density is 20% higher than the noncrystalline density (27).

For crystallization using the metal-chelating lipids, core streptavidin was injected beneath a DOIDA-Cu monolayer. A time sequence of BAM images showing the aggregation process of streptavidin is shown in Fig. 4. The first aggregates appeared 15 min after streptavidin was injected to the final concentration of 150 nM. The aggregates grown beneath a DOIDA-Cu monolayer appear bright on a dark background. A gray scale analysis of these images reveals that the protein density of the phase surrounding the aggregates is negligible. The aggregates are rectangular in shape and show sharp edges. The aggregate size increases as more and more protein adsorbs to the interface, whereas the sharp-edged shape of the aggregates is preserved over time. The aggregates tend to interlock at corner positions, again without inducing a change in their shape.

In contrast to the H-shape of the 2D crystals of streptavidin bound to biotinylated monolayers, copper-bound streptavidin aggregates are rectangular. Our findings that the streptavidin aggregates which formed upon binding to

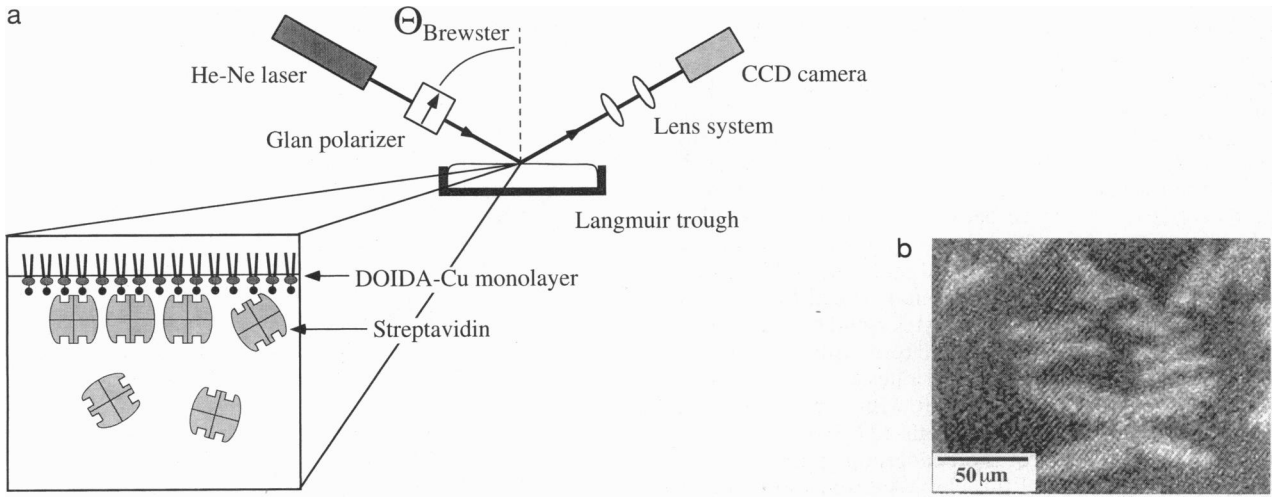

FIG. 3. (*a*) Schematic of BAM. The bare water interface produces no reflection of *p*-polarized light incident at Brewster's angle. When a covering layer even as thin as a molecular monolayer is introduced, *p*-polarized light is reflected, and an image can be created. (*b*) Brewster angle micrograph of streptavidin crystals beneath a biotinylated lipid monolayer (DPPE-X-biotin; Molecular Probes). The H-shape is typical of streptavidin crystals grown on biotinylated-lipid monolayers.

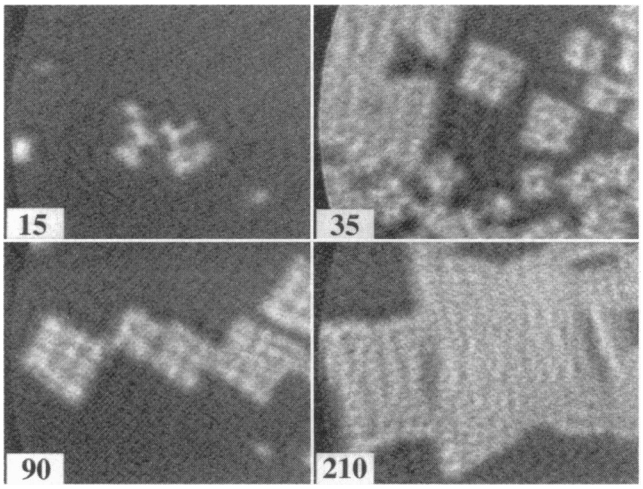

FIG. 4. Time sequence of BAM images of 2D streptavidin aggregation underneath a monolayer of DOIDA-Cu [3 mN/m^2 over 20 mM Mops and 250 mM NaCl (pH 7.8) at room temperature]. Numbers indicate minutes after protein injection. Note the different shape of the aggregates with respect to the H-shaped crystals grown on the biotinylated-lipid monolayer (Fig. 3). The sharp-edged rectangular shape of the domains strongly suggests 2D protein crystals.

DOIDA-Cu monolayers all show the same rectangular shape and that the shape is independent of the aggregate size and the equilibration time, strongly suggest that the aggregates are, in fact, 2D streptavidin crystals. IDA-Cu-bound streptavidin appears to crystallize into a 2D polymorph that is distinct from the biotin-bound form and manifests itself by a rectangular microscopic crystal shape, suggesting altered protein–protein contacts. This is consistent with the ability of streptavidin to crystallize in several polymorphs in two and three dimensions (4, 18). Crystallographic characterization of the 2D copper-bound streptavidin crystals is under way.

Injection of the soluble metal chelator EDTA into the subphase after the streptavidin crystals had formed at the interface caused the protein crystals to disappear within minutes. Routinely used to regenerate IDA-Cu IMAC columns, EDTA competes effectively with the IDA headgroup for copper ions (Fig. 1) and is effective for eluting strongly bound proteins. That the streptavidin crystals are disrupted by EDTA indicates that surface binding requires the presence of copper ions. In fact, no crystals were observed after injection of the same amount of streptavidin underneath a DOIDA monolayer that did not contain Cu^{2+}. In the absence of copper, essentially no protein bound to the interface.

The orientation assumed by streptavidin upon binding to the monolayer depends on the location of the IDA-Cu binding site(s) on the protein surface. Each streptavidin monomer has two histidine residues; His-87 is located close to the biotin binding pocket while the His-127 residue lies on the long side of the barrel at the interface between two subunits, as illustrated in Fig. 5. Two His-127 residues from adjacent subunits come into close contact at the subunit interface and lie on the surface of the protein in a 14-Å deep cleft. The different shape of copper-bound streptavidin aggregates could be explained if the two adjacent His-127 residues were responsible for binding, as monolayer attachment via these residues would be expected to rotate the streptavidin by roughly 90° with respect to binding via biotin. Metal coordination by His-127, however, seems unlikely due to the length of the headgroup spacer (11.5 Å) with respect to the depth of this cleft. A streptavidin mutant in which His-127 is replaced by cysteine (H127C), in fact, showed the same adsorption and crystallization behavior as native streptavidin on DOIDA-Cu monolayers. Thus the two His-87 are left as the most likely sites for interaction with the

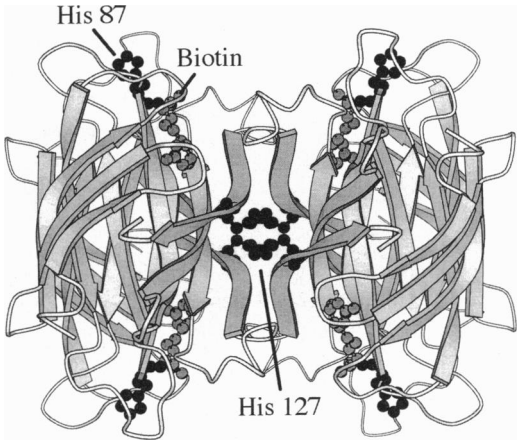

FIG. 5. Structure of the streptavidin tetramer (18) showing the relative locations of the biotin-binding pocket and histidine residues. Biotin and the His-87 residues are located on the "top" and "bottom" of the protein, whereas the His-127 residues lie on the "front" and "back" faces. The image was created using the programs MOLSCRIPT and RASTER3D (28–30).

copper–chelate complexes. Experiments performed with a streptavidin mutant in which His-87 is replaced by Ala (H87A) demonstrate that His-87 is indeed required for streptavidin binding to metal-chelating lipids and the subsequent crystal formation. This mutant shows high affinity for biotin. When injected to a concentration of 250 nM beneath the DOIDA-Cu monolayer, however, H87A streptavidin showed no evidence of binding over a period of 3 hr, as confirmed by a gray scale analysis of the BAM images.

Streptavidin binding to IDA-Cu-derivatized surfaces requires the presence of His-87, but binding occurs only in the absence of biotin. Mature aggregates grown on the DOIDA-Cu monolayer desorbed spontaneously when biotin was injected into the subphase to a total concentration of ≈2.25 μM (15 times molar excess over the streptavidin concentration). In addition, when streptavidin is pre-bound with biotin before injection beneath the DOIDA-Cu monolayer, no protein surface binding is detected. Similar behavior is observed during chromatography on an IDA-Cu column. Fig. 6 shows that apolipoprotein-streptavidin binds rather strongly, requiring ≈40 mM imidazole to displace it. In contrast, streptavidin fully loaded with biotin shows little, if any, affinity for the metal-containing support. We can conclude from these observations that both the disruption of streptavidin crystals

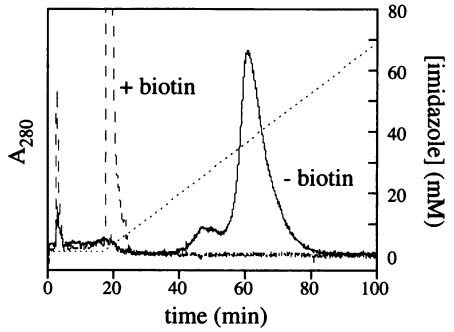

FIG. 6. Chromatogram showing retention of streptavidin in the presence and absence of biotin in metal-affinity chromatography on a IDA-Cu-derivatized support. The protein was eluted with a linear gradient of imidazole (dotted line). In the absence of biotin (solid line), streptavidin is strongly retained on the IDA-Cu column: 40 mM imidazole is required for elution. Streptavidin that has been preincubated with four equivalents of biotin is retained only slightly (dashed line), eluting from the column at the start of the imidazole gradient.

upon addition of biotin and the absence of 2D crystallization of biotin-bound streptavidin are due to inhibition of binding to the IDA-Cu monolayer rather than inhibition of crystallization.

The results reported here indicate that His-87 can coordinate to IDA-Cu only in the absence of biotin. Weber *et al.* (18) report biotin-induced conformational changes. These could render His-87 less accessible for formation of the ternary IDA-Cu protein complex. Alternatively, biotin-induced conformational changes, including hydrogen-bonding between biotin and neighboring residues, could preclude any conformational changes His-87 must undergo for metal binding. Further experiments are under way to clarify the mechanism by which biotin interferes with streptavidin binding to the IDA-Cu lipid monolayer.

2D crystallization of proteins on metal-chelating lipid monolayers via histidine-metal coordination extends the powerful monolayer 2D crystallization technique to virtually any protein with accessible histidines, either natural or engineered. Introducing histidines at specified locations on the protein surface allows control over protein orientation, a major advantage with respect to using polyhistidine tags. Thus a larger range of orientations could be sampled for crystallization, and, in the event that multiple orientations lead to crystallization, 2D electron density maps could be obtained for different protein orientations with respect to the surface plane. In addition to those benefits to structural biology, the ability to form ordered arrays of proteins will facilitate the production of novel devices and functional materials.

W.F. was supported by a Feodor–Lynen fellowship from the Alexander von Humboldt Foundation, W.R.S. by a Biotechnology training grant fellowship from the National Institutes of Health (GM 08437), and D.W.P. by a training fellowship from the National Institute of General Medical Sciences (National Research Service Award 1 T32 GM 08346–01). This research was supported by the National Aeronautics and Space Administration (NAG 8–1149), the Office of Naval Research (N00014–92-J-1178), and the U.S. Army Research Office.

1. Darst, S. A., Ribi, H. O., Pierce, D. W. & Kornberg, R. D. (1988) *J. Mol. Biol.* **203,** 269–273.
2. Kornberg, R. & Darst, S. A. (1991) *Curr. Opin. Struct. Biol.* **1,** 642–646.
3. Blankenburg, R., Meller, P., Ringsdorf, H. & Salesse, C. (1989) *Biochemistry* **28,** 8214–8221.
4. Hemming, S. A., Bochkarev, A., Darst, S. A., Kornberg, R. D., Ala, P., Yang, D. S. C. & Edwards, A. M. (1995) *J. Mol. Biol.* **246,** 308–316.
5. Uzgiris, E. E. & Kornberg, R. D. (1983) *Nature (London)* **301,** 125–129.
6. Furuno, T. & Sasabe, H. (1993) *Biophys. J.* **65,** 1714–1717.
7. Lebeau, L., Oudet, P. & Mioskowski, C. (1991) *Helv. Chim. Acta* **74,** 1697–1706.
8. Lebeau, L., Olland, S., Oudet, P. & Mioskowski, C. (1992) *Chem. Phys. Lipids* **62,** 93–103.
9. Mesini, P., Lebeau, L., Oudet, P. & Mioskowski, C. (1992) *Chem. Phys. Lipids* **63,** 27–35.
10. Kubalek, E. W., Le Grice, S. F. J. & Brown, P. O. (1994) *J. Struct. Biol.* **113,** 117–123.
11. Arnold, F. H. (1991) *Bio/Technology* **9,** 151–156.
12. Ng, K., Pack, D. W., Sasaki, D. Y. & Arnold, F. H. (1995) *Langmuir* **11,** 4048–4055.
13. Dietrich, C., Schmitt, L. & Tampe, R. (1995) *Proc. Natl. Acad. Sci. USA* **92,** 9014–9018.
14. Johnson, R. D., Todd, R. J. & Arnold, F. H. (1996) *J. Chromatogr. A* **725,** 225–235.
15. Shnek, D. R., Pack, D. W., Sasaki, D. Y. & Arnold, F. H. (1994) *Langmuir* **10,** 2382–2388.
16. Pähler, A., Hendrickson, W. A., Gawinowicz Kolks, M. A., Argarana, C. E. & Cantor, C. R. (1987) *J. Biol. Chem.* **262,** 13933–13937.
17. Hendrickson, W. A., Pähler, A., Smith, J. L., Satow, Y. Merritt, E. A. & Phizackerly, R. P. (1989) *Proc. Natl. Acad. Sci. USA* **86,** 2190–2194.
18. Weber, P. C., Ohlendorf, D. H., Wendoloski, J. J. & Salemme, F. R. (1989) *Science* **243,** 85–88.
19. Weber, P. C., Wendoloski, J. J., Pantoliano, M. W. & Salemme, F. R. (1992) *J. Am. Chem. Soc.* **114,** 3197–3200.
20. Darst, S. A., Ahlers, M., Meller, P. H., Kubalek, E. W., Blankenburg, R., Ribi, H. O., Ringsdorf, H. & Kornberg, R. D. (1991) *Biophys. J.* **59,** 387–396.
21. Chilkoti, A., Tan, P. H. & Stayton, P. S. (1995) *Proc. Natl. Acad. Sci. USA* **92,** 1754–1758.
22. Chilkoti, A., Schwartz, B. L., Smith, R. D., Long, C. J. & Stayton, P. S. (1995) *Bio/Technology* **13,** 1198–1204.
23. Todd, R. J., Johnson, R. D. & Arnold, F. H. (1994) *J. Chromatogr. A* **662,** 13–26.
24. Martell, A. E. & Smith, P. M. (1974) *Critical Stability Constants* (Plenum, New York), Vol. 6.
25. Hönig, D. & Möbius, D. (1991) *J. Phys. Chem.* **95,** 4590–4592.
26. Henon, S. & Meunier, J. (1991) *Rev. Sci. Instrum.* **62,** 936–939.
27. Frey, W., Schief, W. R. & Vogel, V. (1995) *Langmuir* **12,** 1312–1319.
28. Kraulis, P. J. (1991) *J. Appl. Crystallogr.* **24,** 946–950.
29. Bacon, D. J. & Anderson, W. F. (1988) *J. Mol. Graphics* **6,** 219–220.
30. Merritt, M. A. & Murphy, M. E. P. (1994) *Acta Crystallogr. D* **50,** 869–873.